



HAL
open science

OXIDATION MECHANISMS OF LOW ENERGY-HIGH FLUX NITRIDED ODS FeAl INTERMETALLIC ALLOY

Fernando Pedraza, Jean-Luc Grosseau-Poussard, J.F Dinhut

► **To cite this version:**

Fernando Pedraza, Jean-Luc Grosseau-Poussard, J.F Dinhut. OXIDATION MECHANISMS OF LOW ENERGY-HIGH FLUX NITRIDED ODS FeAl INTERMETALLIC ALLOY. *Materials at High Temperatures*, 2005, 22, pp.283-286. 10.3184/096034005782744209 . hal-00512787

HAL Id: hal-00512787

<https://hal.science/hal-00512787>

Submitted on 1 Sep 2010

HAL is a multi-disciplinary open access archive for the deposit and dissemination of scientific research documents, whether they are published or not. The documents may come from teaching and research institutions in France or abroad, or from public or private research centers.

L'archive ouverte pluridisciplinaire **HAL**, est destinée au dépôt et à la diffusion de documents scientifiques de niveau recherche, publiés ou non, émanant des établissements d'enseignement et de recherche français ou étrangers, des laboratoires publics ou privés.

OXIDATION MECHANISMS OF LOW ENERGY-HIGH FLUX NITRIDED ODS FeAl INTERMETALLIC ALLOY

F. Pedraza, J.L. Grosseau-Poussard, J.F. Dinhut*

LEMMA, Université de La Rochelle, 25 rue Enrico Fermi, 17042 La Rochelle cedex 1, France.

* *corresponding author: fpedraza@univ-lr.fr. Tel.: +33.(0)5.46.45.82.97. Fax.: +33.(0)5.46.45.72.72*

Abstract

Microscopy studies of low energy-high flux nitrided ODS FeAl Grade 3 intermetallic alloy reveal a surface containing a random distribution of protrusions anchored by yttria particles. The cross section analyses show the formation of an outer compact layer containing hexagonal AlN followed by an inner diffusion layer containing AlN and a segregation of α -Fe. The high temperature isothermal oxidation behaviour is subsequently evaluated at 800° C for 24 h. The nitrided layer is observed to induce a change in the oxidation mechanisms compared to the untreated material. As a result of the outer diffusion of Fe a Fe_2O_3 scale is first established at the gas/metal interface, followed by an intermediate α - Al_2O_3 layer. The original substrate also seems to be oxidised to give rise to a spinel layer the oxide/alloy interface.

1.- INTRODUCTION

Upon the high temperature oxidation in air of TiAl intermetallic alloys, nitridation is observed between the oxide scale and the substrate [1,2] improving their oxidation resistance [3,4]. However, after nitridation treatments of the same alloys, detrimental effects occur [5-8]. In Fe_3Al alloys, the oxidation behaviour is worse in air than in pure oxygen due to internal

nitridation below a defective alumina scale [9]. In the present work, a low energy-high flux nitridation treatment at moderate temperature of ODS FeAl Grade 3 has been performed to modify the surface and produce an enrichment in nitrogen of the superficial layer. Upon subsequent oxidation, a beneficial effect is expected.

2.- EXPERIMENTAL PROCEDURE

FeAl40 at% Grade 3 with 15 ppm B, 0.1 wt% Zr and 1 wt% Y₂O₃ dispersion, kindly furnished by CEA/CEREM [10] was obtained by extrusion at 1100°C after mechanical alloying leading to a strong <110> fibre texture and a mean grain size in the micrometer range. The nitridation treatment was performed with a 1.2 keV flux of nitrogen ions (N⁺ and N₂⁺ ions) and a beam current intensity of 1mA.cm⁻². The temperature was fixed at 400°C, and the implantation time was 1 hour to obtain implanted doses of 3.5x10¹⁹ at/cm². Before implantation, a cleaning treatment made of Ar⁺ sputtering was carried out at 1.2 keV and 0.5 mA.cm⁻² for 15 min [11]. Under these experimental conditions, a several microns thick layer containing about 20 at% N was obtained in a stainless steel [12].

The oxidation experiments were performed on specimens (15 mm in diameter, 1 mm thick) mechanically polished down to a final roughness of 0.01 µm and ultrasonically degreased in acetone and rinsed in 99% ethanol. Isothermal oxidation tests were carried out in a SETARAM TG DSC92 analyser. A platinum wire was used to hold the specimen in the furnace and the thermogravimetric measurements were recorded after heating at 50°C/min up to the oxidation temperature under an argon atmosphere. Then, an artificial air (80% N₂-20% O₂) flow was let in the oxidising chamber for 24 h. The mass gain was measured with an accuracy of 1 µg.

Characterisation of the implanted and oxidised samples was undertaken using contact mode atomic force microscopy (AFM) with an Autoprobe CPR (Veeco Instr.), scanning electron microscopy (SEM) in a JEOL JSM-4510 LV coupled with an EDS device and transmission electron microscopy (TEM) in a JEOL-JEM 2010 operating at 200 kV. The TEM cross sections were prepared by polishing with SiC 4000 emery paper down to about 50 μm then bombarded with 3 keV Ar^+ ions in a GATAN PIPSTM 691 using different angles.

3. – RESULTS AND DISCUSSION

Effect of the nitridation treatment

The morphology of the nitrided alloy is shown in Fig. 1. The top view (Fig 1a) is uniform throughout the whole surface, and some porosity is observed as a result of the manufacturing process (powder metallurgy) or because of bubbles arising from the nitridation process as already observed in Ni [13]. AFM observations show ridges pinned by round particles (Fig 1b) composed of Y and O, which can be attributed very likely to the Y_2O_3 dispersion of the intermetallic alloy. The SEM cross section in Fig 1c shows the nitrided layer of about 1.5 μm thick with protrusions at the outer surface due to the deformation induced upon nitridation. Microscopic details can be obtained by using TEM cross section observations (Fig 2). Fig 2a reveals that the nitrided layer is composed of equiaxed grains whereas Fig 2b and 2c give the evolution of this layer showing an outer part composed of Fe, Al and N, and the Fe content increases up to 75at% near the interface layer/substrate. The N-rich top surface is about 1 μm thick and comes from the major inward nitrogen and the outward aluminium diffusion during the implantation process. As a result, the Fe rich interface appears since the enthalpy of formation is in favour of the external formation of AlN [14].

Oxidation tests

Upon a 24 hours oxidation in artificial air at 800°C, the mass gain per surface unit $\Delta m/S$ of the nitrated specimen is about three times that of the untreated material (Fig 3). A rapid increase in $\Delta m/S$ is recorded in a first step for about the first hour of the oxidation process. After a transition stage, a different kinetic is observed. The k_p values (Fig 3b) deduced for the first ($1.3 \times 10^{-2} \text{ mg}^2 \text{ cm}^{-4} \text{ h}^{-1}$) and the second stage ($9.35 \times 10^{-4} \text{ mg}^2 \text{ cm}^{-4} \text{ h}^{-1}$) have to be compared to the value for the untreated material ($5.3 \times 10^{-4} \text{ mg}^2 \text{ cm}^{-4} \text{ h}^{-1}$). It clearly appears that the first oxidation stage occurs in a much faster fashion than the second one. The k_p value deduced from the first part of the oxidation curve is near of the measured values when pure iron is oxidised at 400°C [15]; then this observation could be consistent with the presence of α -Fe detected after the implantation process [16,17]. Conversely, the second parabolic constant is much lower and compares well to the one of the untreated FeAl. This may imply that a similar oxidation mechanism is established for the longest oxidation times, where the formation of alumina is expected. The two stage oxidation of the nitrated FeAl Grade 3 is reinforced by the fact that two subscales are observed after oxidation (Fig 3c). TEM analyses on cross section lead to the results in Fig 4. Indeed, the layered structure of the oxide scale appears: the upper part of the film is Fe-rich and consists of hematite as previously observed by X ray diffraction [18]. The underlying zone is constituted of Al and O consistent with the previous suggestion of alumina and with the X ray results of Dang and al. [18], then the spinel phase FeAl_2O_4 and lastly the nitrated zone of the substrate. All these conclusions deduced from the EDS analysis and from diffraction patterns are in agreement with the oxidation behaviour in two steps. Upon oxidation of the nitrated specimens, diffusion of the different species seems to be clearly enhanced through the faulty structure created upon the implantation process. Therefore, the appearance of a first stage related to the formation of hematite by outward diffusion of Fe is fast followed by a second stage in which the inward diffusion of oxygen occurs giving rise to the Al rich scale. Al is nevertheless somewhat trapped by the hexagonal

AlN phase and therefore, major oxygen inward diffusion brings about the formation of the spinel FeAl_2O_4 at the oxide/substrate interface. This last oxide has already been observed after oxidation of FeAl coatings as an external stable oxide [19]. This could suggest that an epitaxial relation ($2\sqrt{2}$) may develop between FeAl_2O_4 and the FeAl substrate (of lattice parameters 0.815 nm and 0.2897 nm, respectively).

4. - CONCLUSION

Nitridation with low energy-high flux of nitrogen implantation at 400°C induces in FeAl Grade 3 a superficial layer containing α -Fe and AlN. When oxidised at 800°C for 24 h in air, the oxidation resistance of the nitrided alloy shows an important decrease compared with the untreated alloy. Two oxidation stages have been related to microscopic mechanisms. The first and faster is due to the outward diffusion of iron, which gives rise to the top hematite scale. The second, attributed to inner diffusion of oxygen leads to spinel Fe-Al oxide.

5.- ACKNOWLEDGMENTS

The authors are very grateful to Prof. J.P. Rivière and Dr. G. Abrasonis (LMP-CNRS-UMR-6630) for the nitridation experiments.

6.- REFERENCES

1. Haanappel, V.A.C., Sunderkotter, J.D. and Stroosnijder, M.F., The isothermal and cyclic high temperature oxidation behaviour of Ti-48Al-2Mn-2Nb compared with Ti-48Al-2Cr-2Nb and Ti-48Al-2Cr *Intermetallics* **7**, 529-541 (1999).
2. Lee, D.B., Kim, M.H., Yang, C.W. Lee, S.H., Yang, M.H. and Kim, Y.J. The Oxidation of TiB_2 Particle-Reinforced TiAl Intermetallic Composites *Oxid. Met.* **56** (3/4), 215-229 (2001).

3. Wu, J.S., Zhang, L.T., Wang, F., Jiang, K. and Qiu, G.H., The individual effects of niobium and silicon on the oxidation behaviour of Ti₃Al based alloys *Intermetallics* **8**, 19-28 (2000).
4. Pérez, P. and Adeva, P. Improvement of Oxidation Behavior of a Ti–48Al–2Cr Alloy by a Nitridation Treatment *Oxid. Met.* **56** (3/4), 271-285 (2001).
5. Magnan, J., Weatherly, G.C and Cheynet, M.C., The Nitriding Behavior of Ti-Al Alloys at 1000° C, *Met. Mat. Trans.* **30A** 19-29 (1999).
6. Zhao, B., Wu, J., Sun, J. and Wang, F. Effect of nitridation on the oxidation behavior of TiAl-based intermetallic alloys *Intermetallics* **9**, 697-703 (2001).
7. Sun, J., Wu, J.S., Zhao, B. and Wang, F., Microstructure, wear and high temperature oxidation resistance of nitrided TiAl based alloys *Mat. Sci. Eng.* **A329-331**, 713-717 (2002).
8. Zhao, B., Wu, J., Sun, J., Tu, B. and Wang, F., Oxidation kinetics of the nitrided TiAl-based alloys *Mat. Letters* **56** (4), 533-538 (2002).
9. Pint, B.A., Regina, J.R, Prüßner, K., Chitwood, L.D., Alexander, K.B. and Tortorelli, P.F., Effect of environment on the oxidation of ingot-processed iron aluminides *Intermetallics* **9**, 735-739 (2001).
10. Montealegre, M.A., González Carrasco, J.L., Morris-Muñoz, M.A., Chao, J. and Morris, D.G., The high temperature oxidation behaviour of an ODS FeAl alloy *Intermetallics* **8**, 439-446 (2000).
11. Ando, S. Tobe, H. Tahara and T. Yoshikawa, Nitriding of aluminum by using supersonic expanding plasma jets *Vacuum* **65**, 403-408 (2002).
12. Pedraza, F., Grosseau-Poussard, J.L., Abrasonis, G., Rivière, J.P. and Dinhut, J.F., Influence of low energy-high flux nitrogen implantation on the oxidation behavior of AISI 304L austenitic stainless steel, *J. Appl. Phys.* **94** (12),7509-7519 (2003).

13. Matthews, A.P., Iwaki, M., Horino, Y., Satou, M. and Yabe, K., Investigation of the effects of room-temperature nitrogen implantation on the precipitation of aluminium nitride, *Nucl. Inst. Meth. Phys. Res.* **B59/60**, 671-675 (1991).
14. Sanghera, H.K. and Sullivan, J.L., Study of low energy high dose nitrogen implantation in aluminium, iron, copper and gold, *Surf. Interface Anal.* **27**, 678-690 (1999).
15. Rebeyrat, S.: Influence d'un traitement de phosphatation sur le comportement en oxydation haute température et sur la consolidation par compression uniaxiale et frittage de poudres de fer, *PhD Thesis* Université de La Rochelle, France (2002)
16. Pedraza, F., Grosseau-Poussard, J.L. and Dinhut, J.F., Nitridation effects on the oxidation mechanisms of an ODS Fe–Al intermetallic alloy, *Appl. Surf. Sci.* **233**, 35-41 (2004).
17. Pedraza, F., Grosseau-Poussard, J.L. and Dinhut, J.F., Low energy–high flux nitrogen implantation of an oxide-dispersion-strengthened FeAl intermetallic alloy, *Thin Solid Films* **467**, 140-145 (2004).
18. Dang Ngoc Chan, C., Huvier, C. and Dinhut, J.F., Effects of an ion nitriding treatment on the oxidation behaviour of an ODS FeAl alloy, *Surf. Coat. Technol.* **165**, 119-125 (2003).
19. Pérez, F.J., Pedraza, F., Hierro, M.P., Balmain, J. and Bonnet, G., Comparison of the High-Temperature Oxidation of Uncoated and CVD–FBR Aluminized AISI-304 Stainless Steel *Oxid. Met.* **58** (5/6) 563-588 (2002).

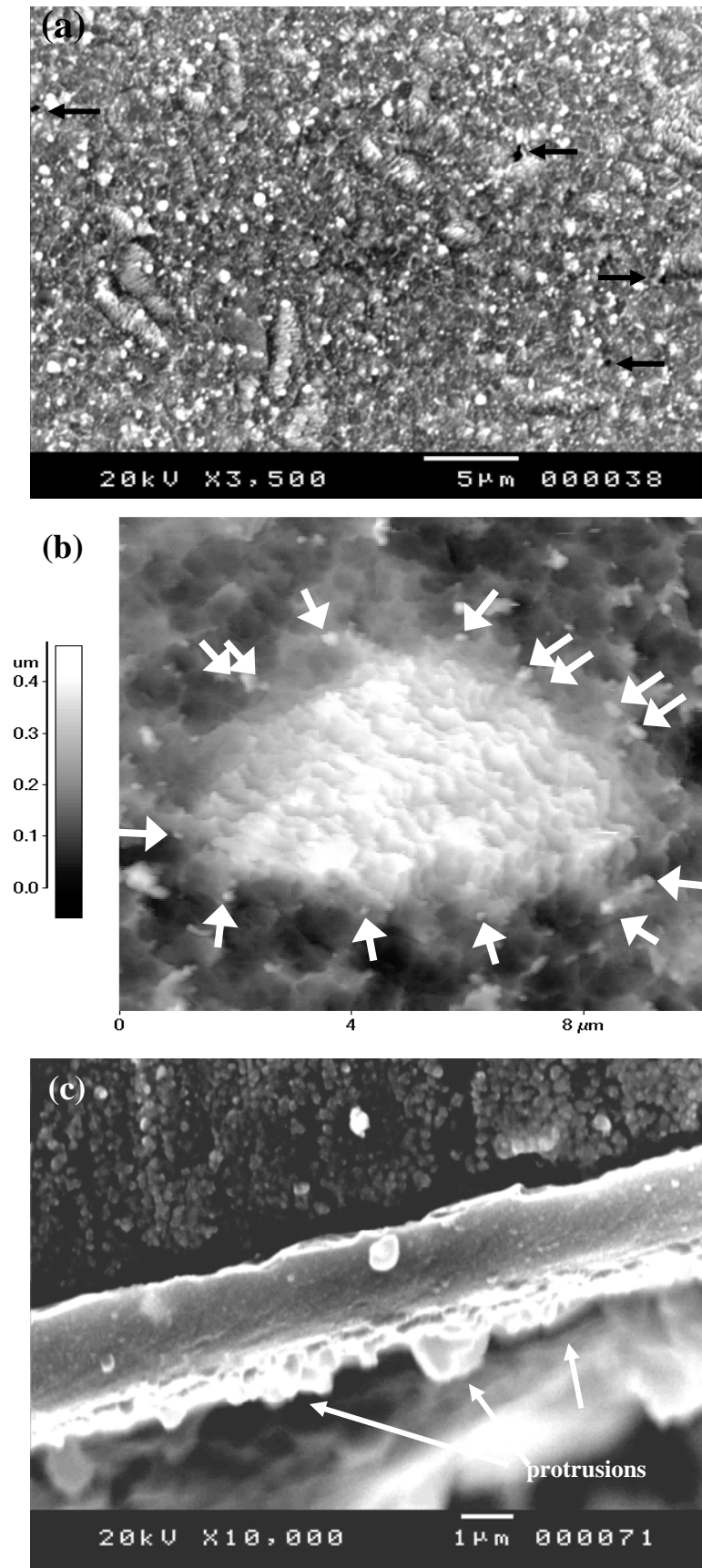


Figure 1.- SEM (a) and AFM (b) surface morphologies showing the induced deformation after nitridation of the ODS FeAl alloy and the pinning effect of Y_2O_3 particles. (c) SEM cross section revealing the compact nitrided layer and the aligned nanograins constituting the extruded alloy.

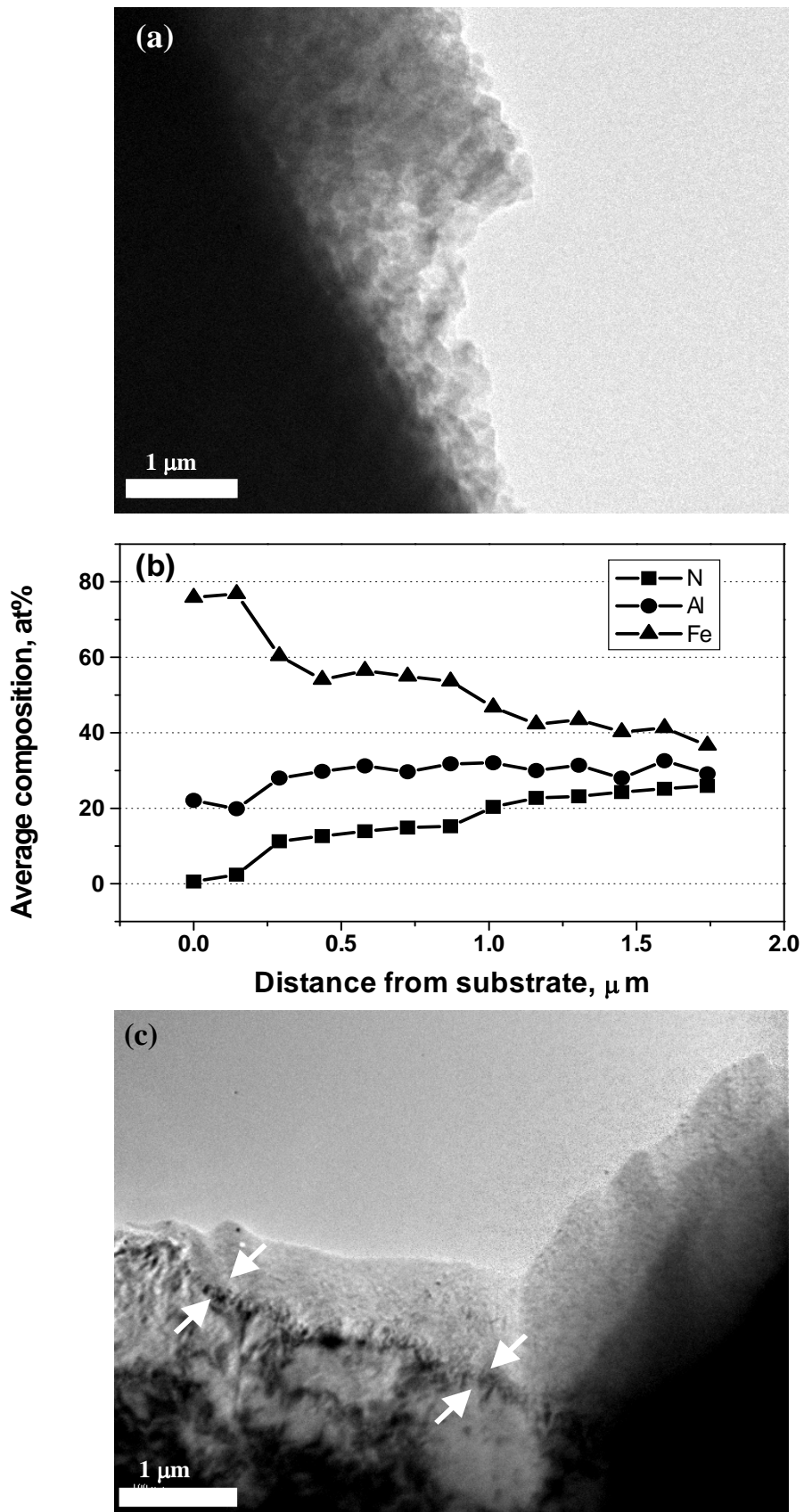


Figure 2.- TEM cross section of the nitrided ODS FeAl intermetallic alloy showing the nanograins composing the nitrided layer (a) and (b) the corresponding EDS composition profile. (c) Detail of the inner diffusion nitrided layer with a-Fe segregation (between arrow marks).

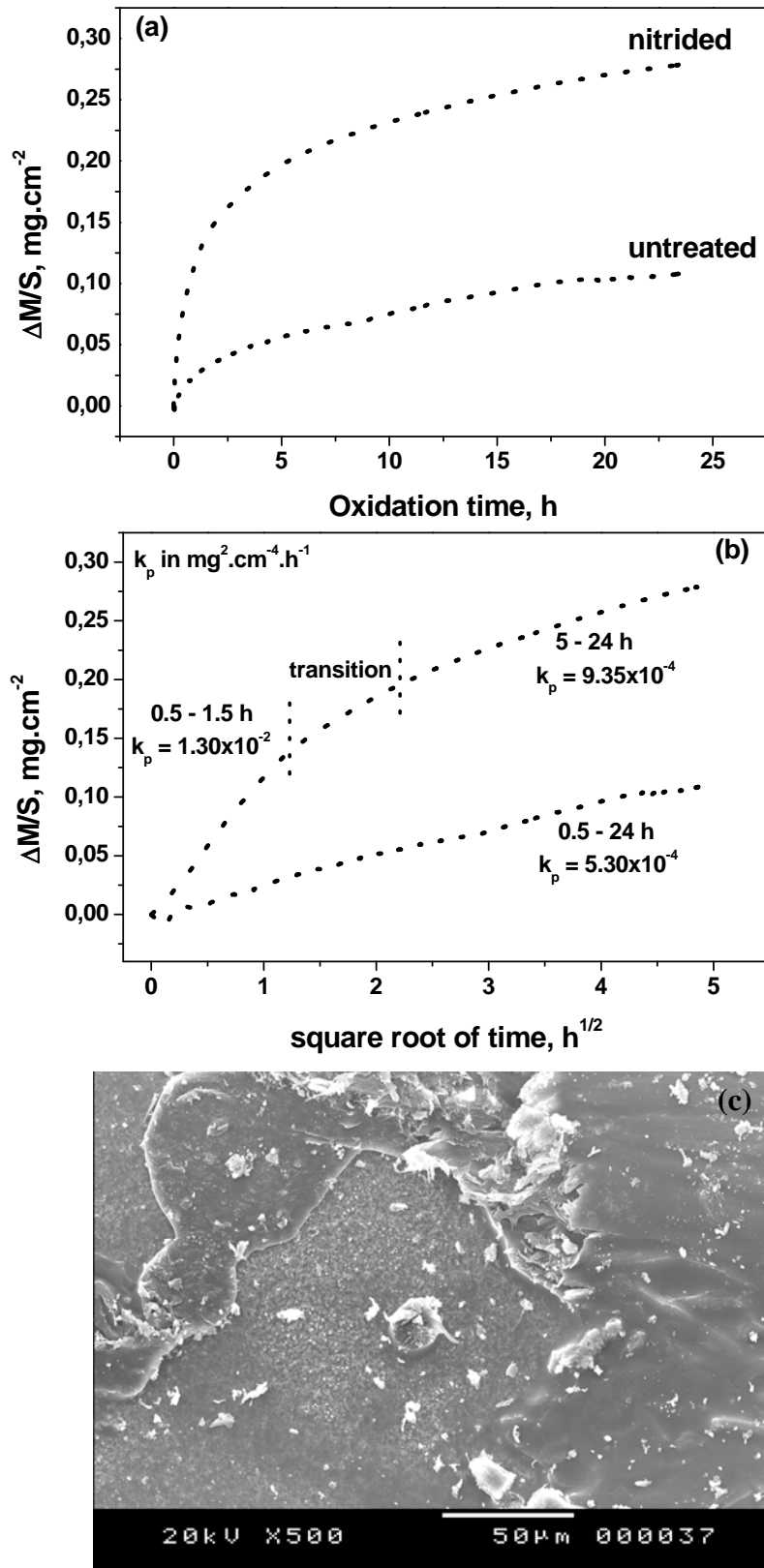


Figure 3.- (a) Mass gain curves of the low energy – high flux nitrided ODS FeAl versus oxidation time at 800° C in synthetic air. The two stage oxidation mechanisms observed as a function of time (b) and the corresponding two oxide sub-scales (c).

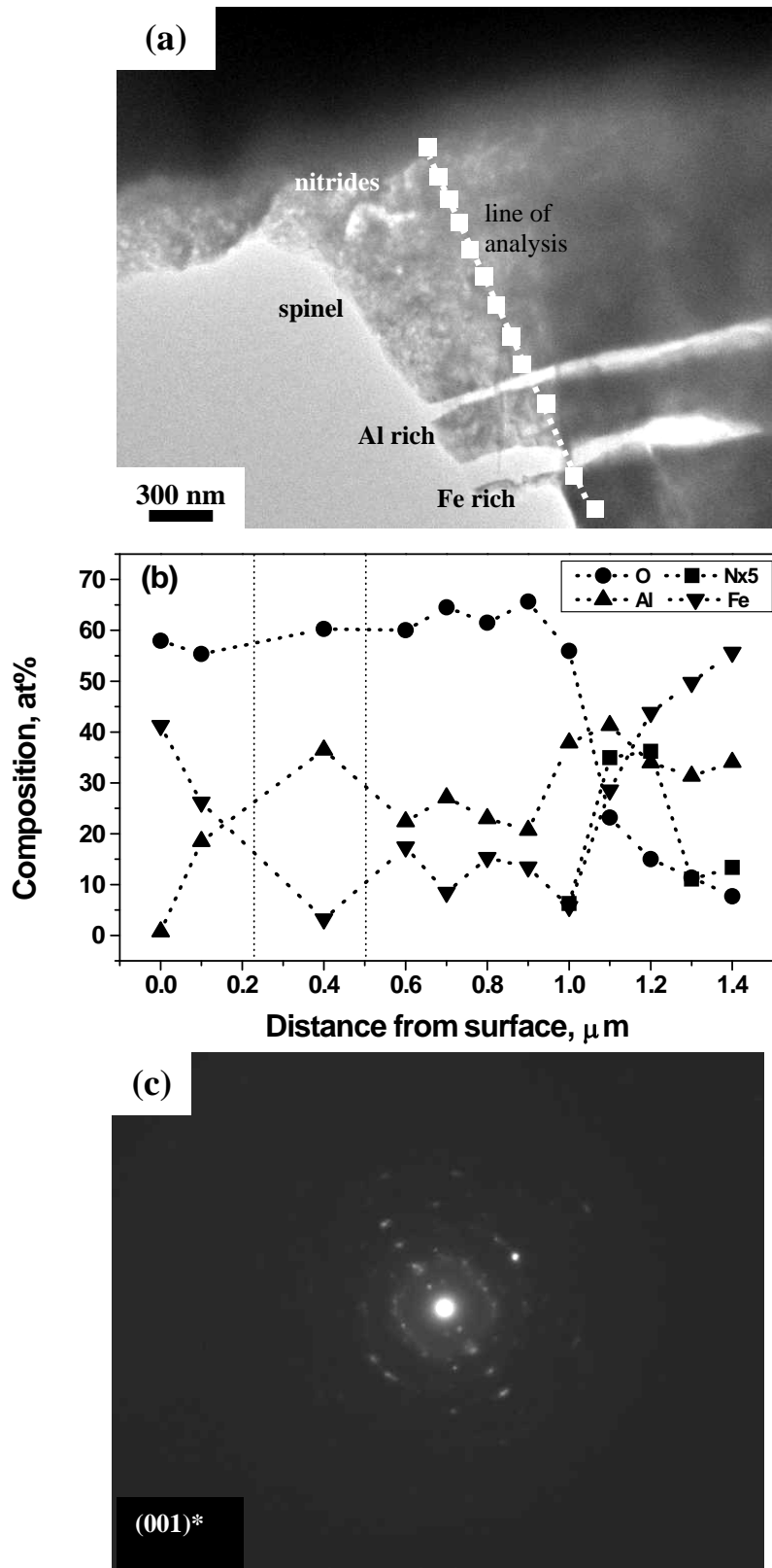


Figure 4.- (a) Bright field TEM image of the stratified oxide scale, (b) EDS microanalyses across all the layers and (c) SADP at the inner scale/substrate interface.